Identity verification using shape and geometry of human hands

Shefali Sharma[1], Shiv Ram Dubey[2], Satish Kumar Singh[2], Rajiv Saxena[3] and Rajat Kumar Singh[2]

[1]*Jaypee University of Engineering and Technology, Guna, India*
[2]*Indian Institute of Information Technology, Allahabad, India*
[3]*Jaypee University, Anoopshahar, India*

This paper has been published by Expert Systems With Applications, Elsevier.
The final publication is available at: http://dx.doi.org/10.1016/j.eswa.2014.08.052.

Citation: Sharma, S., Dubey, S. R., Singh, S. K., Saxena, R., & Singh, R. K. (2015). Identity verification using shape and geometry of human hands. *Expert Systems with Applications*, *42*(2), 821-832.

***Abstract*—** A multimodal biometric system for personal identity verification is proposed using hand shape and hand geometry in this paper. Shape and geometry features are derived with the help of only contour of the hand image for which only one image acquisition device is sufficient. All the processing is done with respect to a stable reference point at wrist line which is more stable as compared to the centroid against the finger rotation and peaks and valleys determination. Two shape based features are extracted by using the distance and orientation of each point of hand contour with respect to the reference point followed by wavelet decomposition to reduce the dimension. Seven distances are used to encode the geometrical information of the hand. Shape and geometry based features are fused at score levels and their performances are evaluated using standard ROC curves between false acceptance rate, true acceptance rate, equal error rate and decidability index. Different similarity measures are used to examine the accuracy of the introduced method. Performance of system is analyzed for shape based (distance and orientation) and geometrical features individually as well as for all possible combinations of feature and score level fusion. The proposed features and fusion methods are studied over two hand image datasets, (1) JUET contact database of 50 subjects having 10 templates each and (2) IITD contactless dataset of 240 subjects with 5 templates each. The proposed method outperforms other approaches with the best 0.31% of EER.

***Index Terms*—** Access control, Identity verification, Biometrics, Hand shape, Hand geometry, Wavelet, Score level fusion.

1. Introduction

Biometrics has gained lot of interest among researchers because of its exponentially growing applications in several areas and its being highly reliable and dependable as far as security is concerned. Different physiological and behavioral traits are used for biometric authentication. Hand based biometrics is considered in this research due to its advantages of low cost, low computational complexity, low template size and more user friendly. Uni-modal systems face major problems of noisy data and intra-class variations (Mansoor, Masood & Mumtaz, 2011). Such problems can easily be reduced by developing multimodal biometric systems. Hand shape and geometry are easily integrated with different modalities such as latent palm-print (Dai & Zhou, 2011), fingerprint (Cappelli, Ferrara & Maltoni, 2010), finger geometry (Malassiotis, Aifanti & Strintzis, 2006), palm-vein (Zhou & Kumar, 2011), Finger-Knuckle-Print (Gao, Yang, Qian & Zhang, 2014) to develop multimodal biometric systems for various applications of different specifications. Hand geometry (Ross & Jain, 1999) and hand shape (Su, 2008; Duta, 2009; Ferrer & Morales, 2011) have been developed and investigated in the literature. Recently, researchers have reported various new multi-model biometric systems based on the hand geometry, hand shape and their combinations with other biometrics in literature. Hand shape and hand geometry are widely adopted because these can be easily captured with any image capturing device. Moreover, the JUET database used in this paper are created using a simple document scanner. Basically hand shape characterizes the boundary of the hand (i.e. relation of one point with other points at the silhouettes), whereas, the hand geometry characterizes the relation of one part of the hand with other

part such as relation between the length of fingers, palm, hand etc. The hand shape and hand geometry only requires the contour of the hand as input. It provides more flexibility to the users and also the number of points to be processed (i.e. only contour points) becomes small which decrease the time complexity of the algorithm. The main problem with the hand shape and hand geometry is that the hand contour can differ too much with the movement of the fingers which is solved in this paper by adopting the finger registration concept.

1.1. Motivation and Related Work

The use of hand images for the biometrics verification has become most popular due to their high user acceptance among the available hand-based biometrics such as fingerprint, palm print, hand geometry, palm vein and finger knuckle (Zhang, Zhang, Zhang & Zhu, 2010). Fotak, Koruga & Baca (2012) have explored new trends in hand geometry. They presented contact based hand image features as elastic graph using graph theory and intend to make it contact-less and combine it with handwritten signature in future. After detailed analysis, they mentioned that hand geometry achieves medium security with benefits of low cost, low computations, low storage requirement and user friendly. Accuracy may get affected due to rings, swelling in fingers unless extra precautions during preprocessing are not taken. Contactless hand geometry is emerging as standard biometric in present time due to ease of use. Guo et al. (2012) have proposed a contact-free identification system based on the hand geometry. The authors have selected 13 points in the palm image and finally extracted 34 features from these points and achieved 96.23% of average correct identification rate, but their results may change with the distortion in projection. In contrast to this method, we have utilized the advantages of the shape of hands also which have proved to be a crucial feature along with the geometrical features. Luque-Baena et al. (2013) have analyzed the reliability of geometric features of hand and extracted total 403 features. They used combination of Genetic algorithm (GA) and Local discriminative analysis (LDA) and finally produced 35 features. They reported 4.51% EER over IITD dataset (137 subjects). Whereas, by fusing geometrical features with the shape features at the score level, the performance of the system is improved significantly. A method of automatic recognition based on hand geometry which doesn't need feature extraction before identification is proposed by Polat & Yıldırım (2008). Neural network based on regression is used for authentication of patterns. System has performed well in terms of the False Rejection Rate (FRR) as well as False Acceptance Rate (FAR) for small database. The performance of such systems can be improved in conjunction with the shape features.

In (Kumar, Wong, Shen & Jain, 2003; Kumar, Wong, Shen & Jain, 2006), the authors have proposed palm-print and hand geometry features based multi-modal biometric recognition system to improve the efficiency. Both the biometric features are obtained from single image which is acquired by digital camera. Both have used simple peg-free systems. Palm-print feature reduces the chances of spoofing thus performance of overall system improves. Note that, the proposed method is also multi-model system but all the modalities require only one camera to capture the hand image. In (Kumar et al., 2006), the author has employed fusion of matching score with max rule as compared to fusion at representation level to achieve the better results. In our case also the fusion is carried at the score level, moreover, we adopted a two level score level fusion to increase the performance of the verification system. Kanhanged, Kumar & Zhang (2011a) combined 3-D features with 2-D features of hand geometry to increase the discriminative ability of the features. They integrated 2-D palm-print, hand geometry, 3-D palm-print and finger texture. The authors have not considered the shape of the hand which is an important feature for hand based biometric system. However, they achieved up to 2.3% of EER at the expense of more computing, whereas our system performs better than using only two modalities i.e. shape and geometry of the human hand. Kanhanged, Kumar & Zhang (2011b) presented an algorithm for hand matching whose performance remains stable with large variations in hand pose (i.e. hand pose invariant recognition). 3-D digitizer is used to acquire hand image. Orientations obtained in 3-D space are utilized for normalizing the pose of 2D and 3D hand images. Hand geometry and palm-print features are investigated and used for matching with dynamic fusion. The problem associated with this approach is slow image acquisition, high cost and large size of 3-D scanner which limits its applicability at the public places. Biometric system with fusion of palm texture and hand shape is proposed at feature level by Kumar and Zhang (2006). They investigated various features and derived different feature sets which are compared using

classification schemes of Naïve Bayes, decision trees, K-Nearest Neighbor (k-NN), and SVM. Some more multimodal biometric systems which combine different type of modalities are features of Eigen-finger and Eigen-palm (Ribaric & Fratric, 2005); palm texture and finger texture Amayeh, Bebis, Erol & Nicolescu (2009) and finger vein and finger texture (Kumar & Zhou, 2012) are reported through the published literature. The main problem with these methods are with the more imaging complexity as well as user flexibility. We worked over both type of datasets contact and contactless dataset. The problems associated with the contactless dataset is that the image may become larger if the hand is near to the capturing device and vice versa and also the hand can be placed at any orientation. Some researchers also tackled this problem and worked on the contactless images (Michael et al., 2010; de-Santos-Sierra et al., 2011). In (de-Santos-Sierra et al., 2011), the authors have used the feature points of the fingers and palms of the hand and reported 2.3% EER, whereas we derived shape features from the hand contour and fused it with the hand geometrical features.

Recently, Takeuchi, Manabe & Sugawara (2013) have utilized the hand shape with the handwriting motion in the air to model a mulimodel soft biometric verification system. This method is able to achieve the good verification performance over 10 subjects but it also requires special cameras such as RGB and depth camera which is not desirable for an efficient and low cost person verification system. Obviously, to form the feature vector from the handwriting motion requires more computation which restricts its applicability in real time. Whereas, in our case both type of hand features are extracted from the same image and even preprocessing step is same for both features which reduces the time complexity of the system. The finger nail plates are very first used by the Kumar, Garg & Hanmandlu (2014) for biometric authentication purpose. This method first finds the nail plate ROI of the Index, Middle and Ring fingers from the hand image and then used Haar wavelet and independent component analysis for the feature extraction. This method has used texture based features of nail plate which is more prone to the noises such as nail polish etc. Whereas, in our method, only contour information is used to find the shape and geometrical features so the effect of noise is removed inherently. Yang, Huang, Zhou, & Liao (2014) have used finger vein and finger dorsal texture fusion for person identification. Again to capture theses modalities special cameras are required including infrared camera in contrast to our method only requires a simple camera. Travieso et al. (2014) have developed biometric system based on hand shape using Hidden Markov Model transformation of hand contour which is independent of spectrum range of image. This method is suitable for the low cost identification system but at the same time has not utilized the power of geometrical features which will not require much more processing for the system but the performance can be boosted significantly. Mohd Asaari et al. (2014) have presented the fusion of finger vein and finger geometry to design a mulimodel biometric recognition system. This method is able to achieve 1.78% EER while used a single complex imaging device to capture the finger vein and geometry. There are two drawbacks of this method; the first one is the lesser flexibility to the users and second one is with the use of only fingers which can't be more discriminative as compared to the full hand of the person, moreover, the spoofing in fingers is also easy. Still the researchers are trying to incorporate the finger based biometric system for person authentication (Kumar, 2014).

1.2. The proposed work

In this paper, shape and geometry of the hand images are extracted in a common framework and used to improve the identity verification of the person by fusing shape and geometry modalities at the score level. The algorithm of proposed system involves image acquisition, image preprocessing, hand orientation registration and reference point extraction, finger feature points determination, shape and geometrical feature extraction, fusion of extracted features at score level and finally hand verification. Hand shape features are encoded in two ways: one finds the distance map while another finds the orientation map of the hand silhouette. We have applied 1-D wavelet decomposition over both shape features (i.e. distance and orientation) to transform into the more distinctive features and selected only most discriminative features for both distance and orientation. We also calculated the hand geometry features by finding the length of the fingers as well as palm of the hand. The matching scores are computed using each modality (i.e. using distance based shape features, orientation based shape features and geometry features). The score level fusion is first applied over the scores of distance and orientation based shape features and the fused score

is again fused with the scores of the geometry features. In other words, score level fusion is applied in two steps: first between the scores of the different shape features and second between the fused score of the shape features and score of geometry features. We observed a great amount of improvement due to the fusion of two shape and one geometry features at score level using different fusion schemes. The main advantage with the shape and geometry based fusion is that their mutual correlation is high while providing more flexibility to the users as well as more imaging simplicity.

This manuscript is structured in following way. Section 2 introduces the proposed approach which consists of the mainly reference point extraction, hand orientation and finger registration and shape and geometry based feature extraction. Section 3 highlights the experimental settings including dataset preparation and score level fusion strategy with the evaluation matrices. Section 4 carried out the experiments over two dataset namely JUET and IITD dataset and reported the performance of the proposed identity verification using shape and geometry of human hands. Finally, section 5 highlights the concluding remarks with future direction.

2. Proposal method

In this section, the introduced approach is described in detail. Fig. 1 illustrates the workflow of the proposed method. First, the preprocessing, hand orientation registration, reference point extraction and finger feature points determination are explained. Then, the shape and geometrical feature description approach are introduced to encode the information in multiple ways only from the contour of the hand image. Experimental settings, evaluation criteria and performance of the proposed approach are explained in further sections.

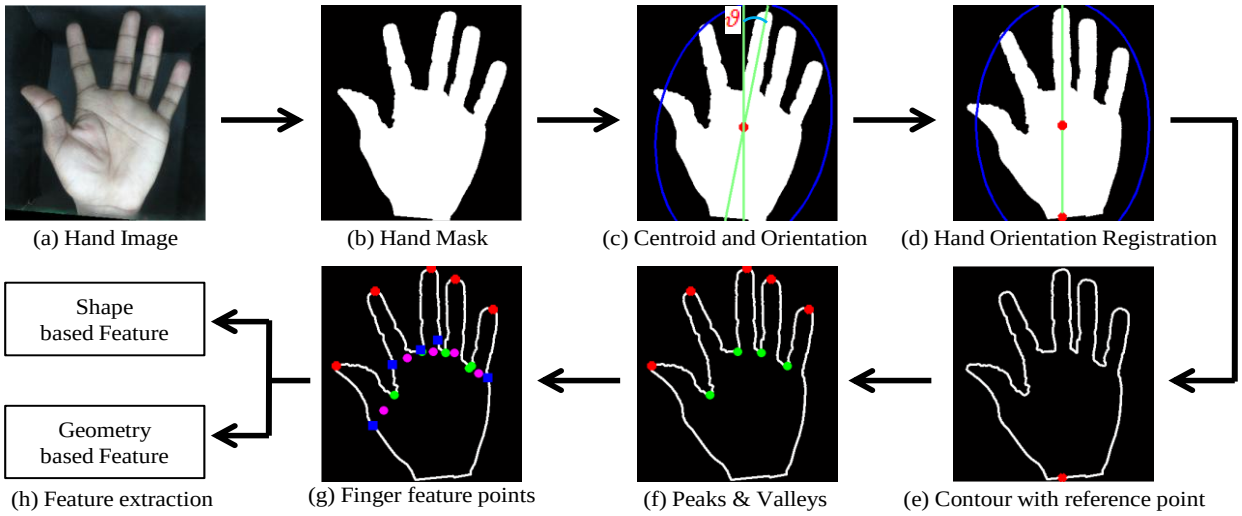

Fig. 1. Workflow of the shape and geometrical feature extraction.

2.1 Preprocessing

To detect the hand region of the images, a preprocessing step is required. The hand images used in this paper are having noise as it is captured using a simple document scanner. The following steps are involved to eliminate the noise as well as background of hand image: first gray scale image is generated from color image; 2-D median filtering with 3×3 filter is applied to get rid of the noise introduced by the scanner which is mainly salt and pepper type noise; the gray scale image is converted into binary image using a threshold; further dilation operation is performed using a diamond structuring element (SE) of size 2 followed by erosion with a square SE of size 3. After all preprocessing steps, a binary image of hand mask is generated. A pre-processed hand mask is generated in Fig. 1(b) for an example hand image of Fig. 1(a). We observed from various preprocessed images that in some cases fingers may be disjoint from the hand mask mainly for some images of the IITD dataset. We have shown it in Fig.

2(b) using an example of Fig. 2(a), in this case the index finger is not attached with the remaining hand mask. We tackled this problem to avoid the intra-class variations and joined the disconnected fingers with the hand mask. The process of joining is illustrated in Fig. 2. First, we find the orientation of disjoint finger and then rotated the whole image such that finger under consideration becomes vertical. Fig. 2(c) shows the hand mask after rotation and the index finger became vertical. Second, we filled the vertical gap between disjoint finger and hand mask by extending the finger in vertical down direction until it connect with the rest hand mask as depicted in Fig. 2(d). Finally, we rotated back the whole image to its original orientation (see Fig. 2(e)).

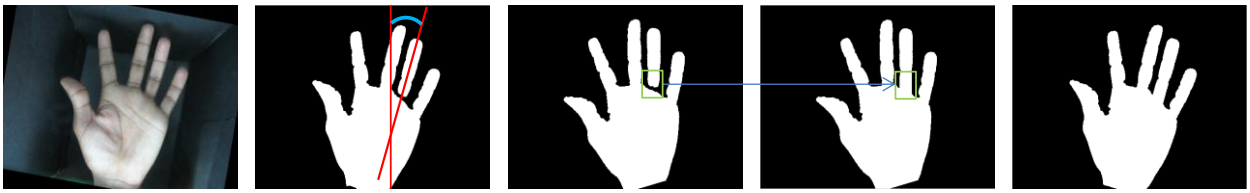

(a) (b) (c) (d) (e)

Fig. 2. Process of joining the disjoint finger to the hand, (a) Original hand image, (b) generated hand mask using pre-processing, the index finger is disjoint from hand, (c) Hand mask is rotated such that index finger became vertical, (d) Index finger is extended such that it became attached with the remaining hand, and (e) The hand mask is rotated to its original orientation back.

2.2 Hand orientation registration

A hand orientation registration is performed in this paper to cope up with the problems associated with the rotation of hand images. Let $\mathfrak{hm}$ is the input hand mask generated after the pre-processing step over which we have to perform hand orientation registration. First, we extract the centroid (μ), orientation of hand (*i.e. orientation of major axis from vertical axis*, θ) and major axis length (Ω) from the region properties of the $\mathfrak{hm}$ measured using *regionprops* function of the MATLAB. The co-ordinate (x_μ, y_μ) of the centriod (μ) can be computed using centre of mass technique as follows,

$$x_\mu = \frac{\sum_{\delta \in hand} x_\delta}{\sum_{\delta \in hand} \mathfrak{hm}} \tag{1}$$

$$y_\mu = \frac{\sum_{\delta \in hand} y_\delta}{\sum_{\delta \in hand} \mathfrak{hm}} \tag{2}$$

The orientation (θ) of the hand mask and also major axis is given as (Weeks, 1996),

$$\theta = 0.5 \tan^{-1}\left(\frac{2\xi_{1,1}}{\xi_{2,0} - \xi_{0,2}}\right) \tag{3}$$

where $\xi_{\alpha,\beta}$ are the central moments and defined as follows,

$$\xi_{\alpha,\beta} = \sum_{\delta \in hand} (x_\delta - x_\mu)^\alpha (y_\delta - y_\mu)^\beta \tag{4}$$

We have centroid and orientation of the hand mask $\mathfrak{hm}$ so the distance between the extreme points but within $\mathfrak{hm}$ on the line passing through μ at an angle of θ from the x-axis will be major axis length (Ω) of the hand mask.

Now the hand orientation registration is done by rotating the image in such a way that the major axis of $\mathfrak{hm}$ becomes vertical. The angle (ϑ) by which $\mathfrak{hm}$ should be rotated in counterclockwise direction to produce the orientation registered hand mask $\mathfrak{hm}'$ is given as,

$$\vartheta = \begin{cases} +90 - \theta, & +90 \geq \theta \geq 0 \\ -90 - \theta, & -90 \leq \theta < 0 \end{cases} \tag{5}$$

The new coordinate of any point $\wp$ of $\mathfrak{hm}$ after rotation w.r.t. μ is defined as,

$$x'_\wp = x_\mu + (x_\wp - x_\mu) \times \cos\vartheta - (y_\wp - \mu) \times \sin\vartheta \tag{6}$$

$$y'_\wp = y_\mu + (x_\wp - x_\mu) \times \sin\vartheta + (y_\wp - \mu) \times \cos\vartheta \tag{7}$$

where, $(x_\wp, y_\wp)$ is the coordinate of any point $\wp$ before rotation and $\wp \in \mathfrak{hm}$. Note that, first we shifted μ of the $\mathfrak{hm}$ at the origin and then rotation is carried out w.r.t. origin and finally we shifted back μ at its original places, so

overall hand mask $\mathfrak{hm}$ is rotated w.r.t. the centoid μ of the original hand mask. Fig. 1(c) depicts the μ, Ω and ϑ of the hand mask of Fig. 1(b) and hand mask is rotated in the Fig. 1(d) such that its major axis became vertical.

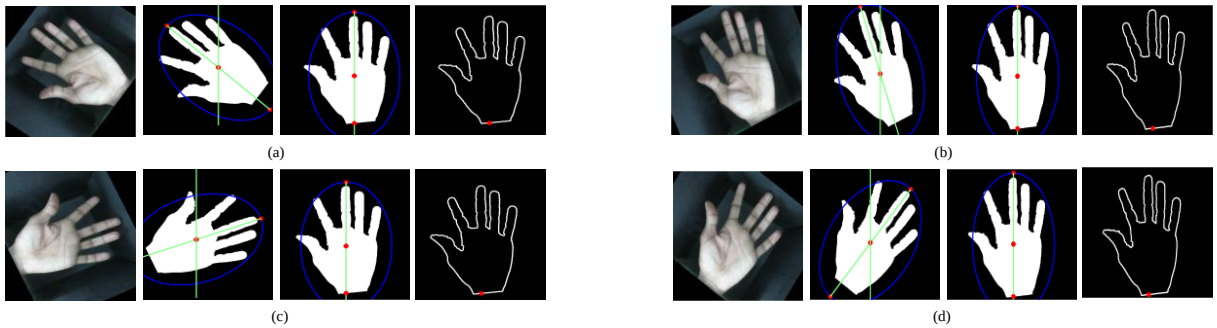

Fig. 3. Robustness of the stable reference point extraction over wrist boundary of the hand.

Algorithm 1. ***The reference point extraction***

```
Input:    Image (I) having registered hand mask (hm'),
          Centroid (μ), Row number (x), Column number (y)
Output:   Reference point (r)
Initial:  j ← 0, tmp ← [ ]

Begin
    [s1, s2] ← size(I)
    For i ← 1 : s1
        If I(i, y_μ) == 1  (i.e. if the value of I(i, y_μ) is 1, where I is the binary image)
            j ← j + 1
            tmp(j) ← i
        end
        x_r ← maximum(tmp)
        y_r ← y_μ
    end
    return (x_r, y_r)
end
```

2.3 Extracting reference point

The further processing requires a stable reference point (r) in the hand to achieve the translation invariance and to detect the peaks and valleys of the fingers accurately. We considered a point at the wrist boundary as a stable reference point because the points of the wrist boundary are the least affected by the rotation of the hands. As depicted in Fig. 1(d), the point of intersection of hand's major axis passing through the centroid μ of the hand with the wrist boundary line is considered as the stable reference point r. The stability and robustness of the reference point extraction are shown in Fig. 3, where reference points are extracted for the 4 images which are rotated by 60^o and 30^o in both clockwise and counterclockwise direction. The reference point extracted in each case is stable and not affected by the rotation of the image. The pseudocode to extract the coordinate of the reference point is given in algorithm 1.

2.4 Finger feature points extraction

In this section, first we find the peaks and valleys of the fingers and then find the two composite valleys for each peak and finally the feature points of each finger are extracted. To calculate the 5 peaks of the fingers and 4 valleys between the fingers, we generated a distance map. The maxima and minima of the distance map are the peaks and

valleys. Let r is the extracted stable reference point at the wrist line of hand with co-ordinate (x_r, y_r) and b_r^{cw} is the boundary of the hand contour traced from the reference point r in clockwise direction. Note that b_r^{cw} is the set of co-ordinates of boundary pixels and its length are same as the number of boundary pixels (N). The Euclidean distance ($\eth$) map of each boundary pixel from the reference point is calculated as,

$$\eth_i = \sqrt{\left(x_r - x_{b_r^{cw}(i)}\right)^2 + \left(y_r - y_{b_r^{cw}(i)}\right)^2} \qquad \forall\ i \in [1, N] \tag{8}$$

where, $(x_{b_r^{cw}(i)}, y_{b_r^{cw}(i)})$ is the co-ordinate of i^{th} boundary pixel in clockwise direction from the reference point r and N is the total number boundary pixels over hand contour.

The $\eth$ map for each boundary pixel is shown in the Fig. 4(b) for the example of Fig. 4(a). In this paper, we used reference point over wrist line instead of using hand centroid because the distances of boundary pixels near about the hand wrist boundary from the reference point are lowest and will not affect the peak and valley determination of the fingers as shown in Fig. 4(b). The five peaks denoted by p_j for $j = 1, 2, \dots, 5$ are the peaks of thumb, index, middle, ring and little fingers respectively where p_j are identified as the local maxima at the index Γ_{p_j} of the distance map. The first peak p_1 represent the thumb peak because the distance map is calculated in clockwise direction from reference r. The four valleys are denoted by v_j for $j = 1, 2, \dots, 4$ are the valleys between the fingers thumb and index, index and middle, middle and ring and ring and little respectively where v_j are identified as the local minima at the index Γ_{v_j} of the distance map. The peaks and valleys are superimposed over the hand contour in Fig. 4(c). The coordinates of p_j and v_j are $\left(x_{b_r^{cw}(\Gamma_{p_j})}, y_{b_r^{cw}(\Gamma_{p_j})}\right)$ and $\left(x_{b_r^{cw}(\Gamma_{v_j})}, y_{b_r^{cw}(\Gamma_{v_j})}\right)$ respectively. It should be noted that except peak p_5, we have a corresponding valley at the right side of each peak i.e. v_j is the pair with p_j for $j = 1, 2, \dots, 4$. In this paper, we have used v_4 as v_5 also (i.e. $v_5 = v_4$). Now we have $\{p_j, v_j\}$ as the peak valley pair for $j = 1, 2, \dots, 5$ (i.e. for each finger).

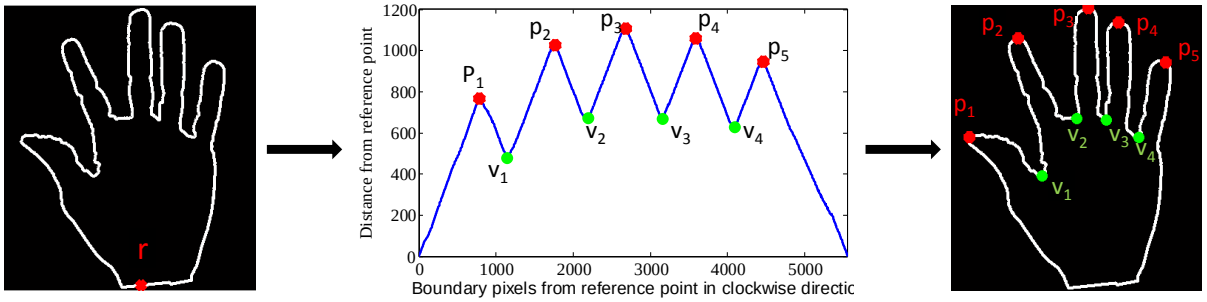

(a) (b) (c)

Fig. 4. Example of finger's peak and valley detection, the red and green marker represent the peaks and valleys respectively, (a) hand contour with reference point, (b) the distance of each point of the contour from the reference point, and (c) detected 5 peaks and 4 valleys of fingers.

In order to extract the finger feature points, we required one more valley points for each finger in composite direction. The index Γ_{c_j} of composite valley c_j corresponding to the valley v_j is extracted using the indexes of p_j and v_j as,

$$\Gamma_{c_j} = \begin{cases} \Gamma_{p_j} - (\Gamma_{v_j} - \Gamma_{p_j}), & \Gamma_{p_j} < \Gamma_{v_j} \\ \Gamma_{p_j} + (\Gamma_{p_j} - \Gamma_{v_j}), & \Gamma_{p_j} > \Gamma_{v_j} \end{cases} \qquad \forall\ j \in [1,5] \tag{9}$$

The coordinate of the points c_j will be $\left(x_{b_r^{cw}(\Gamma_{c_j})}, y_{b_r^{cw}(\Gamma_{c_j})}\right)$.

We have one end point of each finger in form of the peak p_j and calculated another end point m_j from the two composite valleys v_j and c_j of each finger. Let (x_{m_j}, y_{m_j}) is the co-ordinates of m_j which is defined as,

$$x_{m_j} = \left(x_{b_r^{cw}(\Gamma_{v_j})} + x_{b_r^{cw}(\Gamma_{c_j})}\right)/2 \quad \text{and} \quad y_{m_j} = \left(y_{b_r^{cw}(\Gamma_{v_j})} + y_{b_r^{cw}(\Gamma_{c_j})}\right)/2 \qquad \forall\ j \in [1,5] \tag{10}$$

where $\left(x_{b_r^{cw}(\Gamma_{v_j})}, y_{b_r^{cw}(\Gamma_{v_j})}\right)$ and $\left(x_{b_r^{cw}(\Gamma_{c_j})}, y_{b_r^{cw}(\Gamma_{c_j})}\right)$ are the co-ordinates of v_j and c_j. Note that v_j and c_j lies on the contour of the hand whereas m_j lies inside the hand.

Fig. 5(a-e) shows the extracted composite valleys c_j (in blue color) with peaks p_j (in red color) and valleys v_j (in green color) for $j = 1, 2, \ldots, 5$ corresponding to the Thumb, Index, Middle, Ring and Little fingers respectively. The calculated end points m_j (in magneta color) for each finger are shown in Fig. 5(f) for an example of hand image of Fig. 4(c). So, finally at the end of this step we have hand contour with reference point and four features of each finger i.e. peak (p_j), two composite valleys (v_j and c_j) and middle of valleys (m_j).

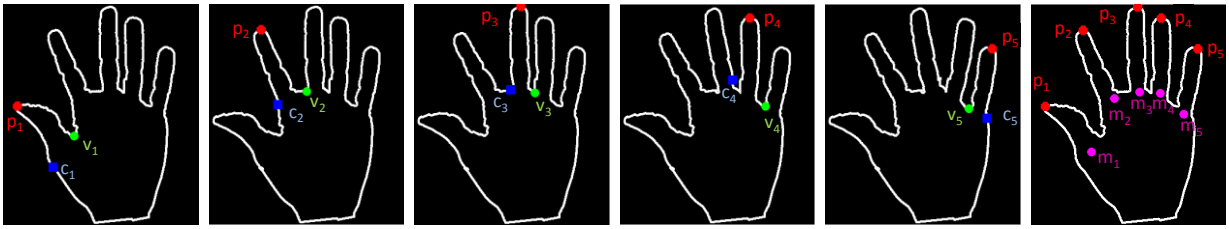

(a) (b) (c) (d) (e) (f)

Fig. 5. (a-e) Finger composite valley points extracted for the thumb, index, middle, ring and little finger respectively and (f) mid-point of the valley and composite valley extracted for each fingers; the peaks, valleys, composite valleys and the mid-point of the valleys and composite valleys are shown in the red, green, blue and magneta color.

2.5 Extraction of Shape features

The shape features are extracted in three steps after knowing the finger feature points. In the first step, the finger registration is performed to achieve the finger rotation invariance; in the second step, distance and orientation maps are generated from the reference point and updated hand contour; in the third step, wavelet decomposition is applied over distance and orientation maps to generate the distance and orientation features.

2.5.1 Finger registration

We worked over the unconstrained hand images which may have the fingers at different orientations that facilitate more user friendly image capture systems. The shape features of hand having fingers at varying orientations are more prone to produce the incorrect result. To avoid this situation, a finger registration is performed in this paper to align the fingers at a particular orientation. Let ω_j is the orientation of j^{th} finger after finger registration for $j = 1, 2, \ldots, 5$. The values of ω_j are considered from the vertical axis in counter-clockwise direction and given as,

$$\omega_j = \begin{cases} +60, & j = 1 \\ +30, & j = 2 \\ +10, & j = 3 \\ -10, & j = 4 \\ -20, & j = 5 \end{cases} \tag{11}$$

The angle ψ_j by which j^{th} finger should be rotated in clockwise direction to perform finger registration is given as,

$$\psi_j = \omega_j - \phi_j \tag{12}$$

where, ϕ_j is the current orientation of the j^{th} finger and calculated from the co-ordinates of the m_j and p_j and defined as,

$$\phi_j = \tan^{-1}\left(\frac{y_{m_j} - y_{b_r^{cw}(\Gamma_{p_j})}}{x_{m_j} - x_{b_r^{cw}(\Gamma_{p_j})}}\right) \tag{13}$$

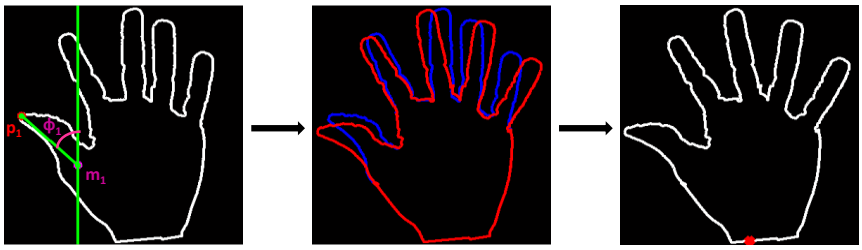

(a) Contour with known finger feature points (b) Finger alignments at particular orientations (c) Updated contour with reference point

Fig. 6. Extraction of distance and orientation features by taking wavelet decomposition of distance and orientation map of hand shape respectively.

Let $\left(x_{\rho_j^\gamma}, y_{\rho_j^\gamma}\right)$ is the co-ordinate of the pixel ρ^γ at j^{th} finger's boundary where ρ_j^γ covers the full boundary of the j^{th} finger starting from $b_r^{cw}(\Gamma_{c_j})$ to $b_r^{cw}(\Gamma_{v_j})$, where $\rho_j^\gamma \subset b_r^{cw}$.

$$x'_{\rho_j^\gamma} = x_{m_j} + \left(x_{\rho_j^\gamma} - x_{m_j}\right) \times \cos\psi_j - \left(y_{\rho_j^\gamma} - y_{m_j}\right) \times \sin\psi_j \tag{14}$$

$$y'_{\rho_j^\gamma} = y_{m_j} + \left(x_{\rho_j^\gamma} - x_{m_j}\right) \times \sin\psi_j + \left(y_{\rho_j^\gamma} - y_{m_j}\right) \times \cos\psi_j \tag{15}$$

where, $\rho_j^\gamma \in [\Gamma_{c_j}, \Gamma_{v_j}]$ and $j \in [1,5]$. The process of finger registration using above mentioned procedure over an example hand image of Fig. 1 is illustrated in Fig. 6(a-b). The final contour with reference point is shown in Fig. 6(c) for same example.

2.5.2 Distance and orientation map

The finger boundaries of hand contour are now updated after finger registration. Note that the reference point is still same as it was previously because wrist boundaries are not changed whereas the centroid of the hand is changed. It means our reference point is more stable than the centroid. Here, we generate the distance map $d\mathcal{P}$ and orientation map $o\mathcal{P}$ using reference point r and updated boundary b'^{cw}_r, where b'^{cw}_r is the coordinates of each pixel of the updated contour traced from r in clockwise direction (i.e. $(x'_{b'^{cw}_r(i)}, y'_{b'^{cw}_r(i)})$ is the i^{th} co-ordinate of b'^{cw}_r). The distance map $d\mathcal{P}$ of each boundary pixel from the reference point is calculated as,

$$d\mathcal{P}(i) = \sqrt{\left(x'_r - x'_{b'^{cw}_r(i)}\right)^2 + \left(y'_r - y'_{b'^{cw}_r(i)}\right)^2} \qquad \forall\ i \in [1, N] \tag{16}$$

where, (x'_r, y'_r) is the co-ordinate of r which is same as (x_r, y_r) used previously and $(x'_{b'^{cw}_r(i)}, y'_{b'^{cw}_r(i)})$ is the coordinate of i^{th} boundary pixel in clockwise direction from the reference point r (i.e. $b'^{cw}_r(i)$) and N is the total number pixels over hand contour.

The orientation map $o\mathcal{P}$ of each boundary pixel from the reference point is calculated as,

$$o\mathcal{P}(i) = 90 + \tan^{-1}\left(\frac{y'_r - y'_{b'^{cw}_r(i)}}{x'_r - x'_{b'^{cw}_r(i)} + \sigma}\right) \qquad \forall\ i \in [1, N] \tag{17}$$

where, $\sigma \approx 10^{-10}$ is a very small number to avoid the division by zero.

2.5.3 Wavelet decomposition

The dimension of $d\mathcal{P}$ and $o\mathcal{P}$ is affected by the varying size of hand and image (i.e. scaling effect) because the number of pixels at hand contour differs. The dimension of $d\mathcal{P}$ and $o\mathcal{P}$ are more for high resolution images and vice-versa. It is observed that increase in the number of pixels of contour will not benefit in the discriminative ability of the $d\mathcal{P}$ and $o\mathcal{P}$. To transform the higher dimension feature into low dimension feature and to select most discriminative features, we used wavelet decomposition because wavelet decomposition is guided in both time and frequency domain (Mallat, 1989). We applied 1-D wavelet decomposition at level 5 using Daubechies-1 wavelet filter over $d\mathcal{P}$ and $o\mathcal{P}$. We selected the first 50 coefficients of the wavelet decomposed $d\mathcal{P}$ and $o\mathcal{P}$ because it is

observed from the experiments that 50 coefficients are sufficient for a good discriminative feature description. We referred the wavelet decomposed dp and $\mathcal{O}p$ as the distance and orientation features in the rest of the paper. So, after wavelet decomposition, we have two shape features distance and orientation each of dimension 50.

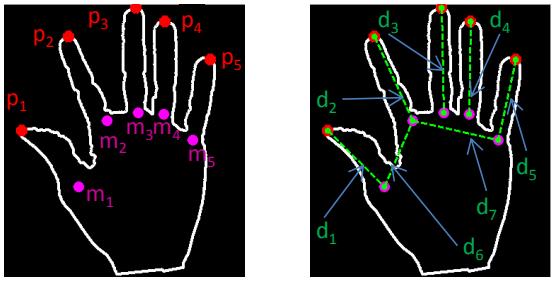

(a) (b)

Fig. 7. Calculation of geometrical features from the finger feature points of the hand contour, (a) Hand contour with finger feature points and (b) 7 distances used as geometrical features.

2.6 Geometrical features

We used the extracted finger feature points i.e. peaks (p_j), and middle of valleys (m_j) to design the geometrical feature description as shown in Fig. 7(a). We calculated 7 distances from 5 finger's end points and finally considered the ratios from these 7 distances in the final description as illustrated in Fig. 7(b). If l number of distances are used then the dimension of final geometrical feature is $l \times (l-1)/2$. The geometrical feature description $g(l \times (l-1)/2)$ using l number of distances is given in algorithm 2. Distance d_j for $j = 1, 2, \ldots, 7$ are defined as,

$$d_j = \begin{cases} \sqrt{(x_{b_r^{cw}(\Gamma_{p_j})} - x_{m_j})^2 + (y_{b_r^{cw}(\Gamma_{p_j})} - y_{m_j})^2}, & j = 1,2,3,4,5 \\ \sqrt{(x_{b_r^{cw}(\Gamma_{p_2})} - x_{b_r^{cw}(\Gamma_{p_1})})^2 + (y_{b_r^{cw}(\Gamma_{p_2})} - y_{b_r^{cw}(\Gamma_{p_1})})^2}, & j = 6 \\ \sqrt{(x_{b_r^{cw}(\Gamma_{p_5})} - x_{b_r^{cw}(\Gamma_{p_2})})^2 + (y_{b_r^{cw}(\Gamma_{p_5})} - y_{b_r^{cw}(\Gamma_{p_2})})^2}, & j = 7 \end{cases} \quad (18)$$

3. Experimental settings

In this section, first we discuss about the acquisition of hand image dataset then we present the score level fusion scheme and hand verification performance evaluation characteristics.

Algorithm 2. Construction of geometrcal feature vector

Input: d_i for $i = 1, 2, \ldots, l$
Output: $g\left(l \times \frac{l-1}{2}\right)$
Variables: a, b, tmp
Initial: $tmp \leftarrow 0$ and $g \leftarrow [\,]$
Begin
  For $a \leftarrow 1 : (l-1)$
    For $b \leftarrow (a+1) : l-1$
      $tmp \leftarrow tmp + 1$
      $g(tmp) \leftarrow d_a/d_b$
    end
  end
  return g
end

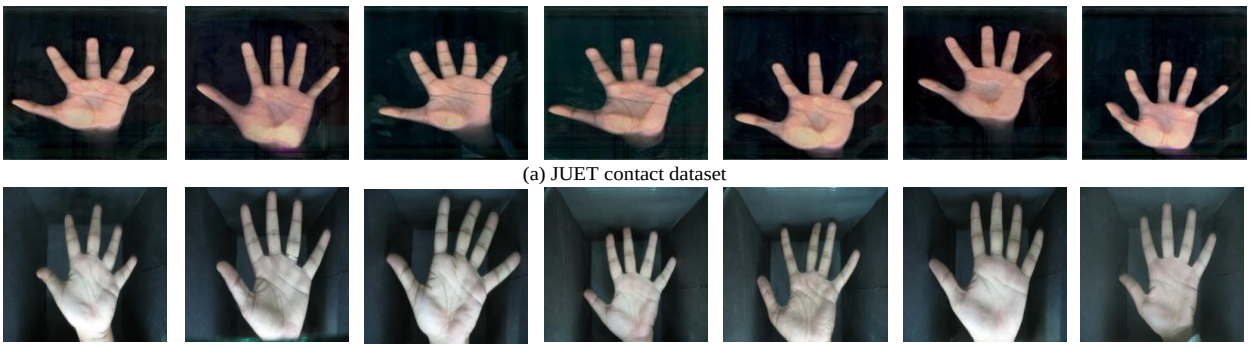

(a) JUET contact dataset

(b) IITD contactless dataset

Fig. 8. Some example images of the JUET dataset.

3.1 Data set acquisition

We have collected the right hand images of our colleagues using a very low cost scanner device to form a hand dataset. Total 50 people are asked to provide 10 images of right hand totaling 500 images. We selected 5 best images of each person to avoid any cropping effect because proposed algorithm is invariant to only translation, rotation and scaling, thus our dataset consists of 250 images (5 images from 50 subjects). In another session, we also collected 5 images from each 100 subjects (totaling 500 images). The use of low cost scanner for image acquisition requires better preprocessing due to more presence of noise (some example images of dataset are shown in Fig. 8).

3.2 Score fusion and verification

Genuine and imposter scores are the distance between the features of the hands of same person and different persons respectively. We matched each image pairs of the same person to find the genuine scores and thus a total 50×5×4/2=500 genuine scores are generated. To generate the imposter scores, the first image of each person is collected and scores are generated for each pair of it and thus a total 50×49/2=1225 imposter scores are generated. We generated the genuine and imposter scores for distance and orientation based shape features as well as geometrical features. The score level fusion is applied on both genuine and imposter scores in two levels.

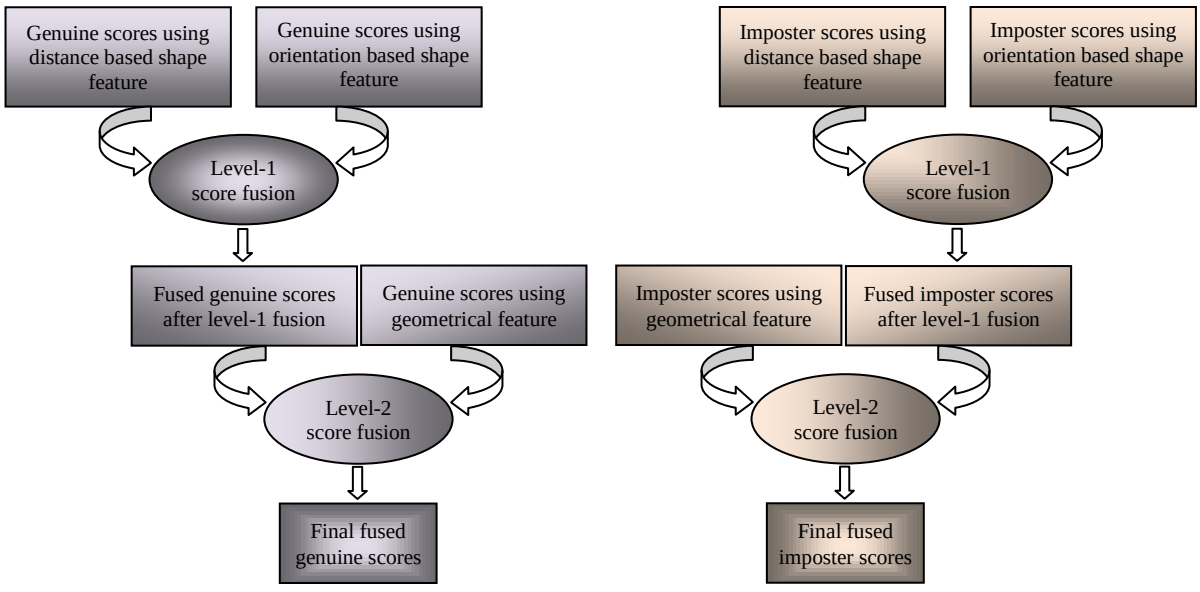

Fig. 9. Two level score fusion of genuine and imposter scores for the identity verification using shape and geometrical features.

In first level we fused the genuine and imposter scores of the distance based shape features with the genuine and imposter scores of the orientation based shape features and computed the genuine and imposter scores after level 1 fusion. In the second step the genuine and imposter scores obtained after first level fusion are again fused with the genuine and imposter scores of the geometrical features respectively to get the final fused genuine and imposter scores. This is also illustrated in the Fig. 9 using level-1 and level-2 score fusion.

Verification results are reported in terms of the True Acceptance Rate (TAR), False Accept Rate (FAR), Equal Error Rate (EER) and decidability index (DI). The TAR is measured as the number of occurrences when genuine images are matched correctly, whereas, FAR is the measurement of the number of occurrences when imposter images are matched falsely. EER is the point where FAR and FRR are equal, where FRR is the False Reject Rate and measured on the basis of number of false rejections of genuine matches and also given as,

$$FRR = 1 - TAR \tag{19}$$

DI is the measurement of the distances between the genuine and imposter scores on basis of mean as well as standard deviation of both scores and defined as (Ramalho et al., 2012),

$$DI = (|\mu_g - \mu_i|) / ((\sigma_g^2 + \sigma_i^2)/2)^{0.5} \tag{20}$$

where, the genuine and imposter score means are represented by μ_g and μ_i respectively and the genuine and imposter scores standard deviations are represented by the σ_g and σ_i. For better verification system, TAR, FAR, EER, and DI should be maximum, minimum, minimum and maximum respectively.

4. Results and Discussion

We present the identity verification results using distance and orientation features individually first in this section and then present the fusion result. We compare the results in terms of ROC curve obtained by the score and feature level fusion of the distance and orientation features. Finally, we compare the hand verification performance with some state-of-the-art methods.

4.1 Results over JUET dataset

We performed the experiments with different similarity measures such as L1, Earth mover distance (Emd), Euclidean, Cosine, Chi-square (chisq or χ^2) and modified hausdorff distance (Mhd) (Piotr's Matlab Toolbox, 2012; Yoruk et al., 2006). The results in terms of EER and DI are presented in Table 1 and Table 2 for distance and orientation features respectively using different similarity criteria and it is found that both the shape features performs better in the case of L1 similarity measure as EER is minimum and DI is maximum for it. We used only 50 wavelet coefficients of both distance and orientation features.

Table 1 EER and DI using 50 wavelet coefficients of distance feature for different similarity measures

	Similarity measure					
	L1	Emd	Euclidean	Cosine	χ^2	Mhd
EER	14.20	16.60	17.80	28.20	40.20	27.60
DI	1.44	1.11	1.38	1.10	0.03	0.76

Table 2 EER and DI using 50 wavelet coefficients of orientation feature for different similarity measures

	Similarity measure					
	L1	Emd	Euclidean	Cosine	χ^2	Mhd
EER	0.180	0.236	0.208	0.310	0.240	0.326
DI	1.092	0.712	1.138	1.074	0.068	0.604

We also performed the experiments using only the geometrical features and results are reported in the Fig. 10(a) and Table 3. Three sets of geometrical features are evaluated, g(6) , g(10) and g(21) consists of ratios of 4 finger lengths {i.e. d_1, d_2, d_3 and d_4}, 5 finger lengths {i.e. d_1, d_2, d_3, d_4 and d_5} and all lengths {i.e. d_1, d_2, d_3, d_4, d_5, d_6 and d_7} respectively, where all length are depicted in Fig. 7(b). From ROC curve it is obsereved that the perfomance of the hand verification is improved with increase number of geometrical features. We also tested the performance of g(21) with different similarity measures in Fig. 10(b) and Table 4. It is evident that the best performance is achieved using Chi-square (χ^2) similarity measure (21.8 % EER). Note that the EER using L1 distance is also 21.8 % and the DI using is L1 is also better than χ^2 but the TAR at a fixed FAR is better for the χ^2 distance.

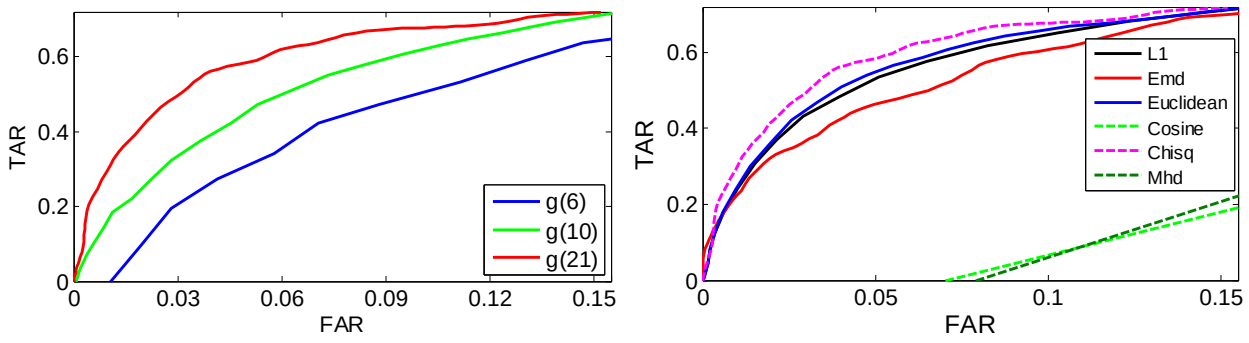

(a) (b)

Fig. 10. ROC plots using only geometrical features with (a) different number of features and (b) different similarity measures.

Table 3 EER and DI using different number of fingers

Feature	g(6)	g(10)	g(21)
Distance	χ^2	χ^2	χ^2
EER	23.60	22.40	21.80
DI	0.61	0.64	0.61

Table 4 EER and DI using geometry feature g(21) with different similarity measures

	Similarity Measure					
	L1	Emd	Euclidean	Cosine	χ^2	Mhd
EER	21.80	23.00	22.20	40.40	21.80	37.40
DI	0.76	0.63	0.76	0.71	0.61	0.47

Table 5 EER and DI using different combinations of genuine and imposter score fusion

	Score fusion strategies								
	pd(d, o), pd(d, o)	sm(d, o), sm(d, o)	mn(d, o), mn(d, o)	ma(d, o), ma(d, o)	mn(d, o), mx(d, o)	mx(d, o), mn(d, o)	sm(d, o), pd(d, o)	pd(d, o), sm(d, o)	mn(pd(d, o), g), mx(sm(d, o), g)
EER	15.20	15.00	15.00	16.40	9.80	25.20	54.60	2.80	0.40
DI	1.13	1.37	1.43	1.21	2.09	0.66	0.37	2.84	3.15

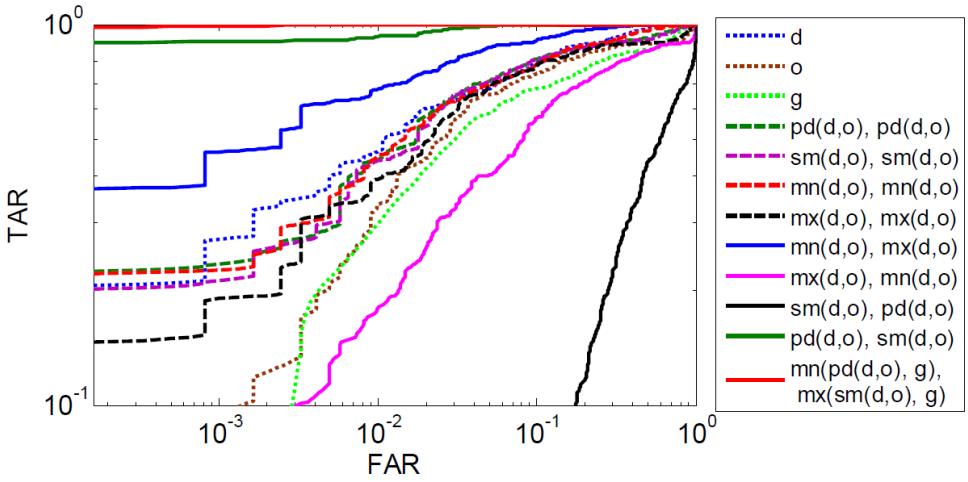

Fig. 11. ROC curve for score level fusion using different combinations of fusion strategies.

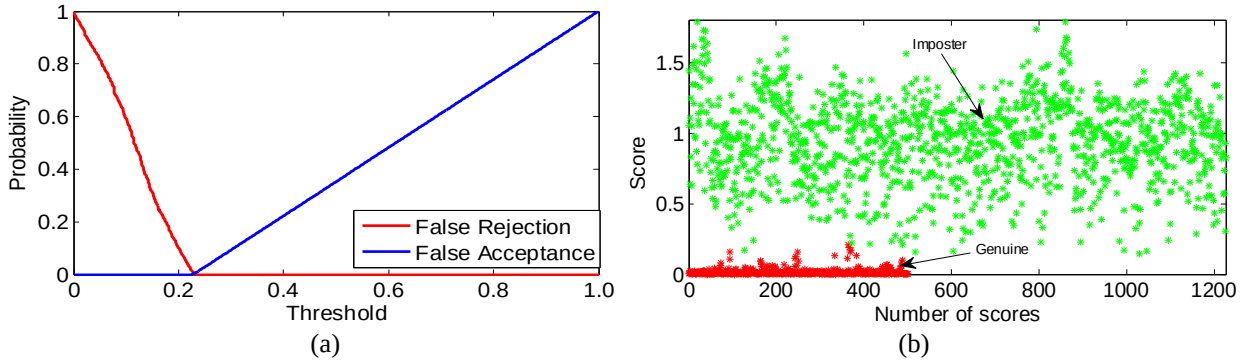

Fig. 12. (a) False rejection (FA) and false acceptance (FA) with different thresholds, and (b) genuine and imposter scores after score fusion of all three modalities.

The score level fusion is incorporated in this paper using the scores of shape distance, shape orientation and geometrical features. We have applied different combinations of strategies for genuine and imposter scores fusion and ROC curves are presented in the Fig. 11. Scores are normalized using min-max normalization rule (i.e. (score-min(score))/(max(score)-min(score))). Multiplication (pd), summation (sm), minimum (mi) and maximum (mx) are the used strategies for score fusion. First we applied the fusion over scores of 'd' and 'o' and it is found that pd(d, o) and sm(d, o) are the best combinations for genuine and imposter score fusion respectively with EER (0.28%) and DI (2.84). We fused the best fusion result of 'd' and 'o' with the scores of 'g' using minimum and maximum rule for genuine and imposter scores. The best EER obtained using score level fusion is 0.4% as depicted in Table 5. The probability of false acceptance and false rejection as function of threshold are depicted in the Fig. 12(a). The FAR at the intersection point is refereed as the EER which is 0.004. The genuine and imposter scores are separated fair enough after score fusion of all three features as illustrated in the Fig. 12(b).

Table 6 EER and DI using different score normalization method

	Score normalization		
	z-score	max-division	min-max
EER	1.26	1.20	0.4
DI	1.51	3.08	3.15

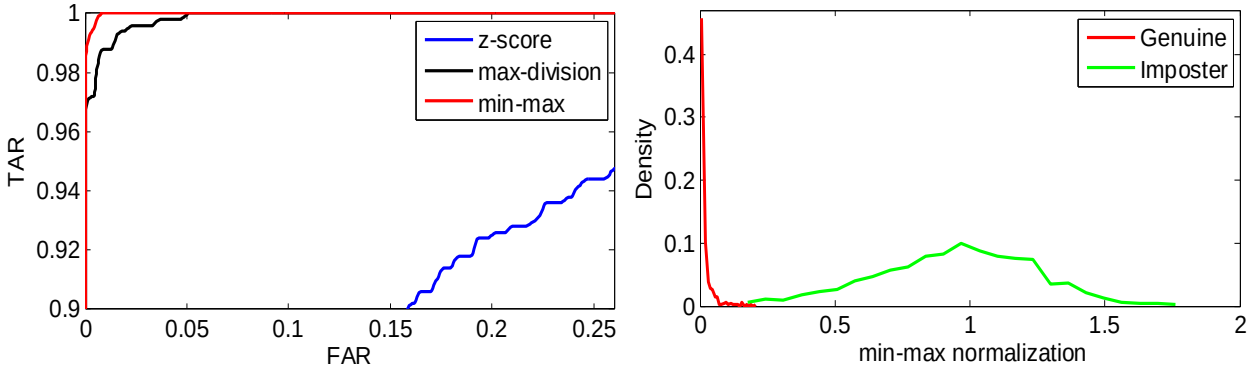

(a) (b)

Fig. 13. (a) ROC plots using different score normalization method, (b) the min-max normalized score density distribution.

Table 7 EER and DI using varying no. of subjects and no. of samples

	No. of subjects × No. of samples		
	case1(50×5)	case2(50×10)	case3(100×5)
EER	0.40	0.31	0.5
DI	3.15	3.21	3.10

We also conducted an experiment with different score normalization methods. Score normalization becomes necessary because the ranges of scores using different modalities are varying and fusing it may lead to an incorrect interpretation. We combined the normalized the scores with z-score, max-division and min-max normalization methods (Mohd Asaari et al., 2014). Fig. 13(a) shows the ROC plots and Table 6 presents the EER and DI values for different score normalization approaches. From Fig. 13 and Table 6, it is observed that z-score normalization is not fit with our algorithm whereas min-max score normalization yields better TAR with least EER (0.4%). Fig 13(b) displayed the frequency of min-max normalized genuine (in red) and imposter (in green) scores respectively. The genuine and imposter are having very less area of intersection in the case of min-max score normalization. The effect of varying number of subjects and number of samples are also tested in Table 7 in terms of the EER and DI. The best EER and DI are 0.31% and 3.21 when the number of subject is 50 with 10 samples each.

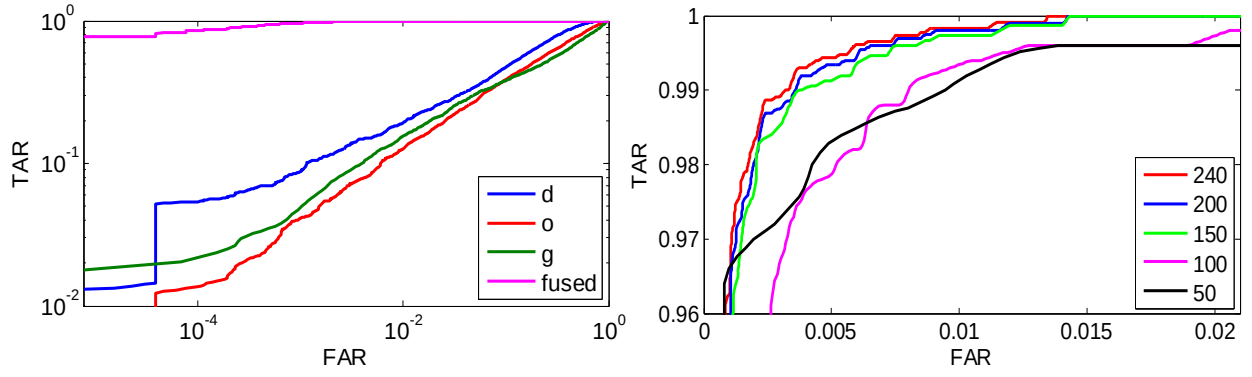

(a) (b)

Fig. 14. (a) ROC curve of score fusion and (b) performance comparison with varying number of subjects.

Table 8 EER (%) and DI using score level fusion

	D	o	g	Fused
EER	26.83	34.06	38.46	0.52
DI	0.94	0.61	0.40	3.16

Table 9 EER (%) and DI with varying no. of subjects of IITD dataset

	Number of subjects				
	240	200	150	100	50
EER	0.52	0.60	0.60	0.80	1.00
DI	3.16	3.16	3.12	3.00	2.79

4.2 Results over IITD dataset

We also tested our approach over widely adopted IIT Delhi hand image dataset (Kumar, 2008). We used right hand images of the IITD dataset which consists of the images of 240 different subjects with 5 samples of each. The results are reported in terms of the ROC curve in Fig. 14(a), and EER and DI in Table 8. It is found that the hand verification performance is improved too much after score fusion of the 'd', 'o' and 'g' features. The EER after score fusion is reduced to the 0.52% with 3.16 DI. The performance are also depicted with varying number of subjects of the IITD dataset in Fig. 14(b) in terms of the TAR and FAR and in Table 9 in terms of the EER and DI. From the results, it is concluded that the performance of proposed approach is better with more number of subjects of IITD datasets as the EER is minimum and DI is maximum for all subjects.

Table 10 Performance comparison with state-of-art in term of Equal Error Rate

Reference	Method	No. of subjects	No. of samples	No. of feat	EER (%)
Travieso et al. (2014)	DHMMK + SVM (UST db.)	287	10	60 DHMM states and 100 edges coding points	0.31
Kumar & Zhang (2006)	Norm. correlation	100	10	16	≈6.81
Michael et al. (2010)	Correlation	50	10	27	4.2
Kanhangad et al. (2011a)	2D Palm-print + 2D hand geometry + Finger texture	177	5	-	0.55
Luque-Baena et al. (2013)	GA-LDA (CASIA db.)	100	6	34	4.64
	GA-LDA (IITD db.)	137	6	35	4.51
de-Santos-Sierra et al. (2011)	Finger features (IITD db.)	235	7	80	2.3
Proposed	Shape + Geometry (IITD db.)	240	5	50+50+21	0.52
	Shape + Geometry (our db.)	50	10	50+50+21	0.31

4.3 Comparison with existing approaches

We compared our method with state-of-art approaches in Table 10 in terms of the EER reported. The best EER reported in other approaches is 0.55% for 2D Palm-print + 2D hand geometry + Finger texture (Kanhangad et al., 2011a), whereas our best EER is 0.31% over our JUET dataset. Using GA-LDA, 4.51% EER is reported in (Luque-Baena et al., 2013) and using 80 features of fingers 2.3% of EER are reported in (de-Santos-Sierra et al., 2011) over IITD dataset whereas proposed method is able to gain 0.52% EER over same dataset using hand shape and geometry features (i.e. total 121 features). From the experimental results and observation, we can say that the introduced identity verification system is an efficient, simpler and low-cost method. Our method is also outperform recent geometrical and shape based personal verification approaches. The introduced method is robust to the different geometrical transformations such as translation, rotation, and scaling.

5. Conclusion

We presented an approach to encode the shape and geometry of the hand from contour information of hand only. Although multi-model system has been developed but do not require separate scanners as in case of other multi-model biometric systems. A method to connect the disjoint fingers in preprocessing is presented. Both shape and geometry features are extracted with respect to a stable reference point at the wrist line of the hand contour. The performance of each feature is tested with different similarity measures. Two shape based features are fused with the geometrical features at the score level to enhance the discriminative ability and efficiency of the identity verification system. The shape and geometry based features used in this paper are highly correlated which benefits in the score level fusion. The two level score fusion also guided the more efficient fusion technique. The proposed approach has used only contour information of the hand which provides more flexibility to the users as compared to the other approaches. Two datasets are considered to evaluate the proposed feature and fusion schemes. The best EER of 0.31% is achieved over JUET dataset of 50 subjects having 10 templates each and 0.52% over IITD dataset of 240 subjects containing 5 images per subject. The proposed system can be used with a simple camera even a document scanner (JUET dataset) and the performance is promising because our preprocessing approaches are also more robust towards the noise as well as geometric transformations as compared to the existing techniques. The experimental studied points out that the proposed method outperforms other approaches and can be utilized effectively for personal verification task.

The future direction of this work includes the consideration of the characteristics of the palm lines. We designed the low cost approach for person verification whereas most of the application requires the systems for the person identification. We will also target to design a low cost, flexible and efficient person identification system. We have considered the contact and contact free databases in this simulation, but in future we will also include the infrared hand images. We will also emphasis to design the more efficient fusion techniques at both representation and score level.

References

Amayeh, G., Bebis, G., Erol, A., & Nicolescu, M. (2009). Hand-based verification and identification using palm–finger segmentation and fusion. *Computer Vision and Image Understanding*, *113*(4), 477-501.

Cappelli, R., Ferrara, M., & Maltoni, D. (2010). Minutia cylinder-code: A new representation and matching technique for fingerprint recognition. *IEEE Transactions on Pattern Analysis and Machine Intelligence*, *32*(12), 2128-2141.

Dai, J., & Zhou, J. (2011). Multifeature-based high-resolution palmprint recognition. *IEEE Transactions on Pattern Analysis and Machine Intelligence*, *33*(5), 945-957.

de-Santos-Sierra, A., Sánchez-Avila, C., del Pozo, G. B., & Guerra-Casanova, J. (2011). Unconstrained and contactless hand geometry biometrics. *Sensors*, *11*(11), 10143-10164.

Duta, N. (2009). A survey of biometric technology based on hand shape. *Pattern Recognition*, *42*(11), 2797-2806.

Ferrer, M. A., & Morales, A. (2011). Hand-shape biometrics combining the visible and short-wave infrared bands. *IEEE Transactions on Information Forensics and Security*, *6*(4), 1305-1314.

Fotak, T., Koruga, P., & Baca, M. (2012). Trends in hand geometry biometrics. In *Proceedings of the Central European Conference on Information and Intelligent Systems* (pp. 323-493).

Gao, G., Yang, J., Qian, J., & Zhang, L. (2014). Integration of multiple orientation and texture information for finger-knuckle-print verification. *Neurocomputing*, *135*, 180-191.

Guo, J. M., Hsia, C. H., Liu, Y. F., Yu, J. C., Chu, M. H., & Le, T. N. (2012). Contact-free hand geometry-based identification system. *Expert Systems with Applications*, *39*(14), 11728-11736.

Guo, X., Zhou, W., & Wang, Y. (2014). Palmprint recognition algorithm with horizontally expanded blanket dimension. *Neurocomputing*, *127*, 152-160.

Kanhangad, V., Kumar, A., & Zhang, D. (2011a). A unified framework for contactless hand verification. *IEEE Transactions on Information Forensics and Security*, *6*(3), 1014-1027.

Kanhangad, V., Kumar, A., & Zhang, D. (2011b). Contactless and pose invariant biometric identification using hand surface. *IEEE Transactions on Image Processing*, *20*(5), 1415-1424.

Kumar, A. (2008). Incorporating cohort information for reliable palmprint authentication. In *Proceedings of the Sixth Indian Conference on Computer Vision, Graphics & Image Processing* (pp. 583-590).

Kumar, A. (2014). Importance of Being Unique from Finger Dorsal Patterns: Exploring Minor Finger Knuckle Patterns in Verifying Human Identities. *IEEE Transactions on Image Processing*, *9*(8), 1288-1298.

Kumar, A., Garg, S., & Hanmandlu, M. (2014). Biometric authentication using finger nail plates. *Expert Systems with Applications*, *41*(2), 373-386.

Kumar, A., Wong, D. C., Shen, H. C., & Jain, A. K. (2003). Personal verification using palmprint and hand geometry biometric. In *Proceedings of the International Conference on Audio-and Video-Based Biometric Person Authentication* (pp. 668-678).

Kumar, A., Wong, D. C., Shen, H. C., & Jain, A. K. (2006). Personal authentication using hand images. *Pattern Recognition Letters*, *27*(13), 1478-1486.

Kumar, A., & Zhang, D. (2006). Personal recognition using hand shape and texture. *IEEE Transactions on Image Processing*, *15*(8), 2454-2461.

Kumar, A., & Zhou, Y. (2012). Human identification using finger images. *IEEE Transactions on Image Processing*, *21*(4), 2228-2244.

Luque-Baena, R. M., Elizondo, D., López-Rubio, E., Palomo, E. J., & Watson, T. (2013). Assessment of geometric features for individual identification and verification in biometric hand systems. *Expert Systems with Applications*, *40*(9), 3580-3594.

Malassiotis, S., Aifanti, N., & Strintzis, M. G. (2006). Personal authentication using 3-D finger geometry. *IEEE Transactions on Information Forensics and Security*, *1*(1), 12-21.

Mallat, S. G. (1989). A theory for multiresolution signal decomposition: the wavelet representation. *IEEE Transactions on Pattern Analysis and Machine Intelligence*, *11*(7), 674-693.

Mansoor, A. B., Masood, H., & Mumtaz, M. (2011). Personal identification using feature and score level fusion of palm-and fingerprints. *Signal, Image and Video Processing*, *5*(4), 477-483.

Michael, G. K. O., Connie, T., Hoe, L. S., & Jin, A. T. B. (2010). Locating geometrical descriptors for hand biometrics in a contactless environment. In *Proceedings of the International Symposium in Information Technology* (Vol. 1, pp. 1-6)

Mohd Asaari, M. S., Suandi, S. A., & Rosdi, B. A. (2014). Fusion of Band Limited Phase Only Correlation and Width Centroid Contour Distance for finger based biometrics. *Expert Systems with Applications*, *41*(7), 3367-3382.

Piotr's Matlab Toolbox (2012). Available from: www.cs.columbia.edu/~mmerler/project/code/pdist2.m.

Polat, Ö., & Yıldırım, T. (2008). Hand geometry identification without feature extraction by general regression neural network. *Expert systems with Applications*, *34*(2), 845-849.

Ramalho, M. B., Correia, P. L., & Soares, L. D. (2012). Hand-based multimodal identification system with secure biometric template storage. *IET Computer Vision*, *6*(3), 165-173.

Ribaric, S., & Fratric, I. (2005). A biometric identification system based on eigenpalm and eigenfinger features. *IEEE Transactions on Pattern Analysis and Machine Intelligence*, *27*(11), 1698-1709.

Ross, A., & Jain, A. K. (1999). A prototype hand geometry-based verification system. In *Proceedings of the 2nd International Conference on Audio and Video Based Biometric Person Authentication* (pp. 166-171).

Su, C. L. (2008). Hand image recognition by the techniques of hand shape scaling and image weight scaling. *Expert Systems with Applications*, *34*(4), 2976-2987.

Takeuchi, A., Manabe, Y., & Sugawara, K. (2013). Multimodal soft biometrie verification by hand shape and handwriting motion in the air. In *Proceedings of the International Joint Conference on Awareness Science and Technology and Ubi-Media Computing* (pp. 103-109).

Travieso, C. M., Ticay-Rivas, J. R., Briceño, J. C., del Pozo-Baños, M., & Alonso, J. B. (2014). Hand shape identification on multirange images. *Information Sciences*, *275*, 45-56.

Weeks, A. R. (1996). *Fundamentals of Electronic Image Processing*. New York: SPIE, pp. 466–467.

Yang, W., Huang, X., Zhou, F., & Liao, Q. (2014). Comparative competitive coding for personal identification by using finger vein and finger dorsal texture fusion. *Information Sciences*, *268*, 20-32.

Yoruk, E., Konukoglu, E., Sankur, B., & Darbon, J. (2006). Shape-based hand recognition. *IEEE Transactions on Image Processing*, *15*(7), 1803-1815.

Zhang, L., Zhang, L., Zhang, D., & Zhu, H. (2010). Online finger-knuckle-print verification for personal authentication. Pattern Recognition, 43, 2560–2571.

Zhou, Y., & Kumar, A. (2011). Human identification using palm-vein images. *IEEE Transactions on Information Forensics and Security*, *6*(4), 1259-1274.